J. Electr. Electron. Mater.
Vol. 39, No. 2, pp. 163-174 March 2026
doi: https://doi.org/10.4313/JEEM.2026.39.2.5
ISSN 1226-7945(Print), 2288-3258(Online)

Tutorial Status Report

X선 회절 기반 $\sin^2\psi$ 기법을 활용한 잔류응력 분석

김환민[1], 우도현[1,2], 시라즈 무함마드[1], 구창영[2], 조성래[1], 안창원[3]

[1] 울산대학교 물리학과
[2] (주)퀀테스
[3] 울산대학교 기초과학연구소

초록: 마이크로 전자기계 시스템(MEMS), 나노 소자, 광전자 및 압전 소자와 같은 첨단 소자 분야에서는 기계적, 전기적, 광학적 성능 향상 및 높은 신뢰성에 대한 요구가 지속적으로 증가하고 있다. 이에 따라 다양한 기능성 박막 소재들이 개발되고 있으며, 특히 높은 압전 특성을 갖는 Pb(Zr,Ti)O_3 (PZT) 박막은 높은 성능의 센서 및 액추에이터 소자 구현을 위한 핵심 소재로 주목받고 있다. 그러나 박막 내 잔류 응력은 소자의 신뢰성, 성능, 수명에 부정적인 영향을 미칠 수 있다. 본 튜토리얼 논문은 $\sin^2\psi$ 방법을 기반으로 한 X선 회절을 이용한 잔류 응력 분석에 대한 실용적이고 단계적인 지침을 제공한다. 대표적인 사례 연구로, 유연한 메탈 호일(Metal foil) 기판 위에 증착된 PZT 박막의 수평 방향의 잔류응력을 정량적으로 분석하였다. 잔류응력 분석을 위해 X선 회절 장비를 활용하였으며, $\sin^2\psi$ 분석법을 적용하여 잔류응력을 평가하였다. 본 $\sin^2\psi$ 분석법은 박막 내부의 잔류응력 분석에 대한 이해를 증진시키는데 기여할 수 있을 것으로 기대된다.

키워드: 잔류응력, X-선 회절, 다결정, 박막, $\sin^2\psi$ 분석법

Residual Stress Analysis Using X-ray Diffraction and the $\sin^2\psi$ Method

Hwan Min Kim[1], Dohyun Woo[1,2], Muhammad Sheeraz[1], Chang Young Koo[2], Sung-Lae Cho[1], and Chang Won Ahn[3]

[1] Department of Physics, University of Ulsan, Ulsan 44610, Korea
[2] Quintess Co., Ltd., Uiwang 16108, Korea
[3] Basic Science Research Institute, University of Ulsan, Ulsan 44610, Korea

(Received January 12, 2026; Revised January 27, 2026; Accepted January 30, 2026)

Abstract: In advanced device technologies such as microelectromechanical systems (MEMS), nanoscale electronics, optoelectronic components, and piezoelectric devices, the demand for enhanced mechanical, electrical, and optical performance together with high reliability continues to grow. In response, a variety of functional thin-film materials have been developed; among them, Pb(Zr,Ti)O_3 (PZT) thin films with high piezoelectric coefficients have emerged as key materials for realizing high-performance sensors and actuators. However, residual stress within thin films can adversely affect device reliability, performance, and lifetime. This tutorial paper provides a practical and step-by-step guide to residual stress analysis using X-ray diffraction (XRD) based on the $\sin^2\psi$ method. As a representative case study, we quantitatively analyze the in-plane residual stress of a PZT thin film deposited on a flexible metal-foil substrate. Residual stress was evaluated using X-ray diffraction (XRD) in combination with the $\sin^2\psi$ method. The present analysis is expected to deepen understanding of residual-stress behavior in thin films and to inform stress-aware design and reliability optimization of PZT-based devices.

✉ **Chang Won Ahn; cwahn@ulsan.ac.kr, cwahn74@gmail.com**
Hwan Min Kim and Dohyun Woo contributed equally to this work.

Keywords: Residual stress, X-ray diffraction, Polycrystal, Thin film, $\sin^2\psi$ method

1. INTRODUCTION

- Polycrystalline thin films are key materials widely used in a broad range of applications, including semiconductors, displays, energy-storage devices, sensors, and micro-electromechanical systems (MEMS), and their industrial demand continues to grow [1-6].
- Thin films can undergo physical damage or property degradation due to residual stress formed within the film as a result of various process-related factors.
- Residual stress can be induced by multiple mechanisms, including mismatch in the thermal expansion coefficients between the substrate and the film, changes in processing temperature, and structural distortion during film growth, and it may lead to mechanical defects such as cracking, delamination, and bending [7-11].
- Residual stress present in polycrystalline thin films has a significant impact on the durability and reliability of the films.
- In addition, polycrystalline thin films exhibit a more complex stress state than single-crystal films due to stress localization associated with the orientation and size of individual grains. Therefore, residual stress analysis is essential for improving the durability and reliability of thin films.
- A variety of measurement techniques have been employed for the quantitative evaluation of residual stress, among which X-ray diffraction (XRD) is widely used because it is nondestructive and enables stress analysis as a function of crystallographic plane orientation. In particular, the $\sin^2\psi$ method can be used to evaluate the in-plane stress in polycrystalline thin films and is therefore regarded as an effective approach for diagnosing and optimizing the mechanical stability of thin films [12].
- In this paper, we introduce the principles of the $\sin^2\psi$ method, a nondestructive XRD-based technique for analyzing residual stress in materials. Using a polycrystal-lline oxide thin film as an example, we present a procedure for evaluating in-plane residual stress. We also discuss the limitations and key considerations associated with the $\sin^2\psi$ method.

2. IMPORTANCE OF RESIDUAL STRESS ANALYSIS IN MATERIALS

- Residual stress refers to the self-equilibrated stress that remains within a material even in the absence of external loading. It directly influences the material properties and structural stability. In particular, excessive tensile or compressive stress in interfacial layers and thin-film layers generated during thin-film deposition and subsequent processing can induce delamination, cracking, and substrate warpage, thereby degrading device durability and lifetime [8].
- Residual stress in thin films can critically affect device reliability. For example, bending or delamination of thin films in MEMS structures can severely impair sensor functionality [13], while in battery electrodes, repeated charge–discharge cycling can lead to stress accumulation that induces expansion and contraction, as well as microcrack formation [14].
- Furthermore, residual stress analysis is extensively applied to a wide range of polycrystalline materials, including hardened steel, welded joints, and ceramics. This measurement technique is utilized to evaluate stresses generated during various manufacturing processes, such as heat treatment, plastic deformation, machining, and welding [15]. Recently, there have been increasing reports on the intentional induction of residual stress through processes like carburizing, nitriding, and shot peening to enhance wear resistance and fatigue life [16]. Therefore, residual stress analysis is essential for improving the lifetime and stability of materials and devices during their development.

3. TYPES OF RESIDUAL STRESS MEASUREMENT TECHNIQUES

3.1 Nondestructive Techniques

- Nondestructive methods for residual stress analysis include X-ray diffraction, neutron diffraction, and Raman spectroscopy.

3.1.1 X-ray Diffraction (XRD)

- X-ray diffraction (XRD) is a widely used nondestructive technique for analyzing crystal structures and lattice spacings and is also extensively applied to residual stress evaluation [17,18]. When X-rays are incident on crystallographic planes in a specimen, diffraction occurs at specific angles according to Bragg's law, enabling precise measurement of the interplanar spacing (d-spacing). XRD offers several advantages, including relatively simple experimental instrumentation, rapid analysis, and high suitability for measuring stresses in thin films or near-surface regions.
- XRD is a representative nondestructive method for measuring stress without damaging the specimen. This enables repeated measurements on the same sample and provides flexibility for potential application during real-time processing.
- XRD can detect nanometer-scale changes in interplanar spacing, offering high sensitivity and spatial resolution. In particular, it allows precise evaluation of near-surface stresses in thin films, making it well suited for thin-film materials analysis.
- XRD can be applied to a wide range of specimens, including thin films, bulk materials, polycrystalline, single-crystal, metals and ceramics, with relatively low sensitivity to substrate geometry.
- XRD enables quantitative stress determination by mathematically interpreting subtle shifts in diffraction angles.
- However, because the X-ray penetration depth is typically limited to only a few micrometers, XRD has inherent limitations for probing stresses deep inside thick materials.

3.1.2 Neutron Diffraction

- In contrast to X-rays, neutron diffraction measures changes in interplanar spacing by irradiating a material with neutrons and offers the major advantage of deep penetration into the interior of a specimen [15,19]. Because neutrons diffract primarily through interactions with atomic nuclei rather than with electrons, internal stresses can be measured nondestructively even in thick specimens with thicknesses of several centimeters. This capability enables three-dimensional mapping of the stress distribution throughout the material and is particularly valuable for evaluating residual stresses in large structures or thick alloy components.
- However, neutron diffraction requires access to high-flux neutron sources, such as research reactors or accelerator-based facilities, which limits instrument availability and increases experimental cost.

3.1.3 Raman Spectroscopy

- Residual stress measurement using Raman spectroscopy is a nondestructive approach that quantitatively evaluates the stress state by analyzing changes in the Raman shift associated with lattice vibrations (phonon modes) [20,21].
- After polishing and cleaning the specimen surface, a monochromatic laser is irradiated onto the sample to generate a scattered-light spectrum; when stress is present, specific Raman peaks shift due to stress-induced changes in the lattice spacing. The magnitude of residual stress can be determined using the correlation between the Raman shift and stress, and in general, the Raman shift tends to increase with increasing stress and decrease as stress is relieved. Raman spectroscopy is particularly advantageous

Table 1. Summary of nondestructive residual stress measurement methods.

Non-destructive method	Penetration depth	Stress component	Advantages	Disadvantages & limitations	Ref.
X-ray diffraction (XRD)	Surface only (few μm)	In-plane stress (biaxial)	High spatial resolution	Limited depth (surface), sensitive to surface roughness	[17,18]
Neutron diffraction	Deep penetration (few cm)	Triaxial stress tensor	Deepest penetration	Long measurement time, low spatial resolution	[15,19]
Raman spectroscopy	Extremely shallow (optical penetration depth)	Local stress tensor (depends on crystal symmetry)	Excellent for micro-scale features (MEMS, thin films), high spatial resolution mapping	Limited materials, difficult for metals (low signal)	[20,21]

because it is nondestructive, safe for operators, and capable of high-spatial-resolution measurements in localized regions, making it effective for residual stress analysis in a wide range of materials, including metal pipes, ceramics, and semiconductor thin films.

3.2 Destructive Techniques

- Destructive approaches for residual stress analysis include the hole-drilling method, the slitting method, and the layer removal method.

3.2.1 Hole-Drilling Method

- The hole-drilling method is a destructive technique for determining residual stress by measuring the strain change that occurs when a small hole is drilled into the surface (Fig. 1(a)) [22-24].
- When a hole of a prescribed depth is introduced into the specimen, part of the pre-existing stress is relieved, leading to deformation in the surrounding region. Strain gauges are attached around the hole to quantify the relieved strain, and the residual stress magnitude is then calculated by coupling the measured strain with an appropriate analytical model.

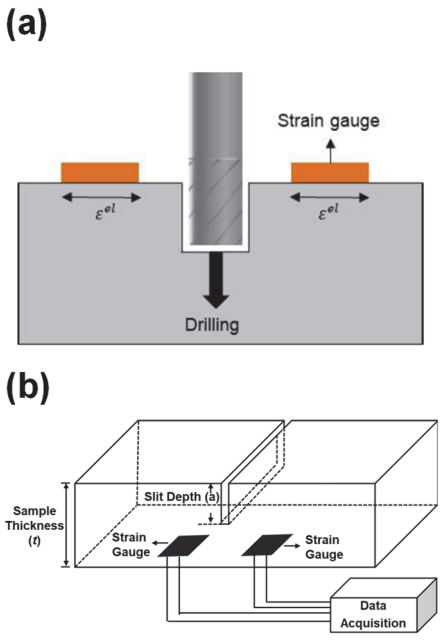

Fig. 1. Schematic illustrations of residual stress measurement using (a) the hole-drilling method and (b) the slitting method. Adapted with permission from [22]. Copyright 2014 Wiley.

- The hole-drilling method is relatively simple and applicable to a wide range of materials. However, it typically provides only an average stress over a localized region, and the specimen is partially damaged due to the drilling process.

3.2.2 Slitting Method

- The slitting method (also known as the crack compliance method) is a destructive technique for determining residual stress by measuring the mechanical stress relief that occurs as a thin slit is progressively introduced into a specimen [25,26].
- Figure 1(b) schematically illustrates the slitting setup, in which a vertical slit is created in the specimen and a strain gauge is attached to the opposite surface. The measurement is performed by machining a narrow slit to a depth a within the total specimen thickness t, typically using wire electric discharge machining (WEDM). As the slit is incrementally deepened, residual stresses within the specimen are progressively relieved, producing small deformations that are recorded by the strain gauge mounted on the back face. By combining the strain data obtained at each depth increment with a compliance matrix or finite element analysis and performing an inverse calculation, the original residual stress distribution through the thickness of the specimen can be quantitatively reconstructed.

3.2.3 Layer Removal Method

- The layer removal method is a destructive technique in which thin layers are continuously or stepwise removed from the specimen surface while the resulting strain or bending is measured at each stage; the through-thickness residual stress distribution is then estimated by back-calculating the original stress field via elastic analysis [27].
- When the surface layer is removed, the stress contained within that layer is released, and the specimen deforms to a new equilibrium state. By recording the deformation response as a function of removal depth, the original stress field can be calculated. Precise layer removal using chemical or electrochemical machining can improve the reliability of the stress analysis.
- However, specimen damage is unavoidable, and the results are highly sensitive to the control of the removal rate, which constitutes a key limitation.

Table 2. Summary of destructive residual stress measurement methods.

Destructive method	Penetration depth	Stress component	Advantages	Disadvantages & limitations	Ref.
Hole-drilling	Surface to a few mm	In-plane stress	Portable equipment, least damage (semi-destructive)	Shallow depth (surface only), risk of induced stress from drilling, requires a flat surface	[22-24]
Slitting method	From surface to core, several mm to cm	Perpendicular to the cut plane	Best for through-thickness profiles in thick components, excellent for measuring stress gradients	Fully destructive (sample not reusable), limited to simple geometries (bars, plates)	[25,26]
Layer removal method	Measured progressively as layers are removed	In-plane stress (distribution along the thickness)	Standard for thin films & coatings, simple principle	Fully destructive, difficult to control removal rate/uniformity, assumes uniform stress across the plane	[27]

3.3 Nondestructive vs. Destructive Techniques

- Because thin films are typically deposited with very small thicknesses, ranging from several tens of nanometers to a few micrometers, mechanical operations such as cutting or drilling can completely damage the specimen. Therefore, nondestructive techniques are generally preferred for residual stress analysis in thin films.
- In contrast, destructive methods are often employed to evaluate through-thickness residual stress distributions in welded structures or to assess the stress state of heat-treated metal components. These approaches are essential when nondestructive techniques cannot provide the required information or when a more detailed stress-profile measurement is needed.
- Overall, nondestructive methods are well suited for residual stress evaluation in high-value thin films, ceramics, and semiconductor devices because they offer high precision while preserving the specimen. Destructive methods, on the other hand, enable reliable stress analysis for depth-dependent stress distributions, complex structures, and non-crystalline materials, where nondestructive approaches may be limited.

4. INTRODUCTION TO THE XRD-BASED $\sin^2\psi$ METHOD

4.1 Fundamental Principle and Mathematical Model

- In conventional XRD measurements (ψ = 0°, Fig. 2(a)), only lattice information along the direction normal to the specimen surface (out-of-plane) is obtained, whereas the lattice response in the in-plane direction cannot be directly evaluated.
- For a specimen subjected to in-plane compressive residual stress, tilting the specimen by varying the ψ angle, as shown in Figs. 2(b) and 2(c), leads to a change in the measured interplanar spacing. Consequently, the XRD pattern exhibits a peak shift, as illustrated in Fig. 2(d). This indicates that the interplanar spacing (d-spacing) varies with the ψ tilt angle. Such ψ-dependent changes in d-spacing can be explained by Bragg's law (Eq. (1)), which accounts for diffraction-peak shifts arising from residual stress.

$$n\lambda = 2d\sin\theta \tag{1}$$

- In Eq. (1), n denotes the diffraction order, λ is the X-ray wavelength, θ is the diffraction angle, and d represents the interplanar spacing of the crystal lattice.

$$d_\psi = \frac{\lambda}{2\sin\theta_\psi} \tag{2}$$

- When the change in interplanar spacing with varying ψ is incorporated into Bragg's law, it can be expressed as Eq. (2). In Eq. (2), d_ψ is the interplanar spacing measured at a specimen tilt angle ψ, and θ_ψ is the diffraction angle obtained at the same ψ tilt.

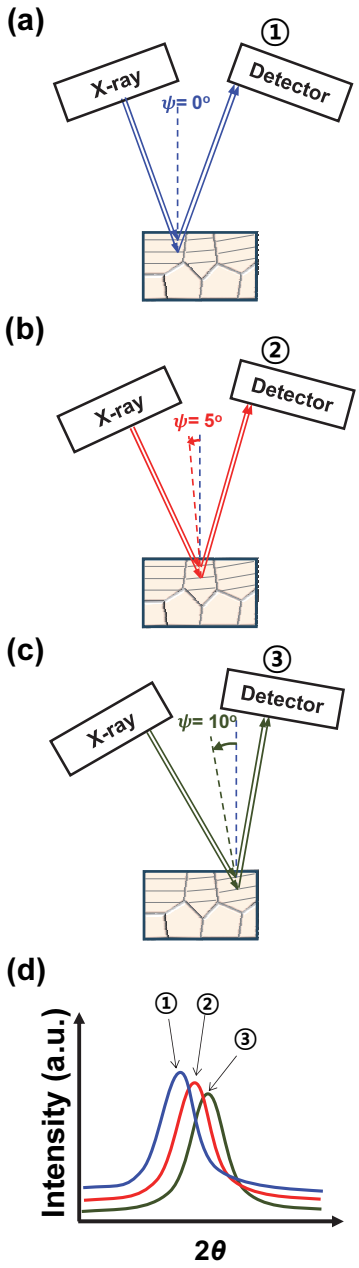

Fig. 2. Schematic illustrations of the X-ray diffraction geometry at ψ angles of (a) 0°, (b) 5°, and (c) 10°, and (d) the corresponding change in the XRD pattern when the specimen is subjected to in-plane compressive stress.

- Therefore, if the XRD peak position (2θ) shifts to higher angles with increasing ψ, as shown in Fig. 2(d), it indicates that the in-plane interplanar spacing is smaller than the out-of-plane spacing. This corresponds to the presence of in-plane compressive residual stress.

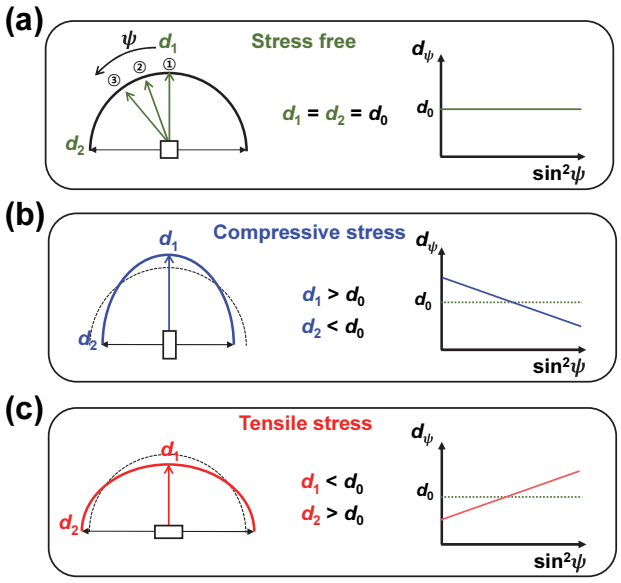

Fig. 3. Schematic illustration of the ψ-dependent change in the interplanar spacing for specimens under (a) stress-free conditions, (b) compressive residual stress, and (c) tensile residual stress [28].

- Figure 3(a) schematically illustrates the ψ-dependent variation in interplanar spacing measured for a stress-free specimen. Because no residual stress is present in the specimen, the XRD peak position does not change with ψ, and the measured interplanar spacing remains constant. Accordingly, the slope of the d_ψ–$\sin^2\psi$ plot is zero.
- Figure 3(b) shows the corresponding schematic for a specimen under in-plane compressive residual stress. In this case, as ψ increases, the measured d value decreases; therefore, the slope of the $d_\psi - \sin^2\psi$ plot becomes negative.
- Figure 3(c) illustrates the case of a specimen under in-plane tensile residual stress. Because d increases with increasing ψ under tensile stress, the slope of the $d_\psi - \sin^2\psi$ plot becomes positive.
- Using the stress-free interplanar spacing d_0 as a reference, the lattice strain ε_ψ can be obtained from d_ψ the interplanar spacing measured at a tilt angle ψ (Eq. (3)). Here, ε_ψ denotes the strain of lattice planes tilted by an angle ψ with respect to the specimen surface.

$$\varepsilon_\psi = \frac{d_\psi - d_0}{d_0} \tag{3}$$

4.2 Stress–Strain Relationship and Equations

- As shown in Fig. 4(a), the three-dimensional stress state of the specimen under a plane-stress assumption can be expressed by Eq. (4). Here, σ_1 and σ_2 represent the stresses along two orthogonal in-plane directions, and ϕ denotes the angle between the in-plane reference axis and the measurement direction [12].

$$\varepsilon_\psi = (\frac{1+\nu}{E}) \cdot \sigma_\phi \cdot \sin^2\psi - \frac{\nu}{E} \cdot (\sigma_1+\sigma_2) \quad (4)$$

- To simplify Eq. (4), Eq. (3) is substituted into ε_ψ, and the in-plane stress is assumed to be isotropic. Under this assumption, $\sigma_\phi = \sigma_1 = \sigma_2 = \sigma$. Accordingly, combining Eqs. (3) and (4) yields Eq. (5). Multiplying both sides by d_0 and rearranging leads to Eq. (6).

$$\frac{d_\psi - d_0}{d_0} = \varepsilon_\psi = \left(\frac{1+\nu}{E}\right) \cdot \sigma \cdot \sin^2\psi - \frac{2\nu}{E} \cdot \sigma \quad (5)$$

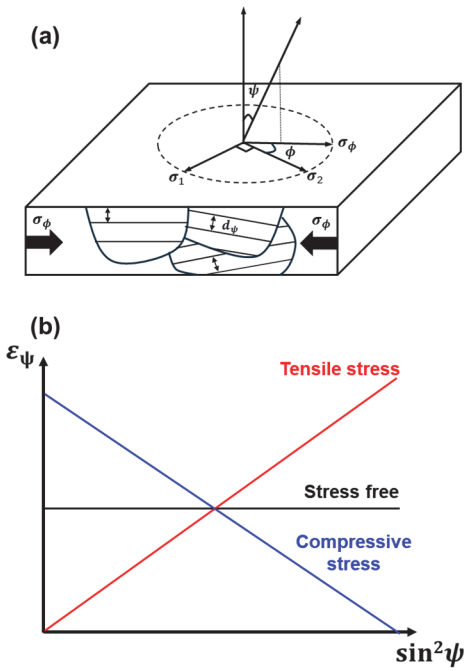

Fig. 4. (a) Schematic diagram for interpreting the stress state in a specimen with residual stress, where σ_ϕ denotes the direction of the residual stress and d_ψ is the interplanar spacing of lattice planes tilted by an angle ψ with respect to the specimen surface. (b) Plot showing the relationship between ε_ψ and $\sin^2\psi$ for residual stress analysis using the $\sin^2\psi$ method.

$$d_\psi = \left[\left(\frac{1+\nu}{E}\right) \cdot \sigma \cdot \sin^2\psi - \frac{2\nu}{E} \cdot \sigma\right] \cdot d_0 + d_0 \quad (6)$$

- Equation (3) can be rewritten as $d_\psi = \varepsilon_\psi \cdot d_0 + d_0$. Substituting this expression into Eq. (6) gives Eq. (7).

$$\varepsilon_\psi \cdot d_0 + d_0 = \left[\left(\frac{1+\nu}{E}\right) \cdot \sigma \cdot \sin^2\psi - \frac{2\nu}{E} \cdot \sigma\right] \cdot d_0 + d_0 \quad (7)$$

- Canceling d_0 from both sides results in Eq. (8).

$$\varepsilon_\psi = \left(\frac{1+\nu}{E}\right) \cdot \sigma \cdot \sin^2\psi - \frac{2\nu}{E} \cdot \sigma \quad (8)$$

- When $\psi = 0^o$, Eq. (8) reduces to Eq. (9).

$$\varepsilon_0 = -\frac{2\nu}{E} \cdot \sigma \quad (9)$$

- ε_0 is a constant term independent of ψ and represents the strain along the direction normal to the specimen surface. Rearranging the expressions therefore yields Eq. (10).

$$\varepsilon_\psi = \left(\frac{1+\nu}{E}\right) \cdot \sigma \cdot \sin^2\psi + \varepsilon_0 \quad (10)$$

- Equation (10) describes the relationship between strain and stress under the assumptions that the specimen is isotropic and that the thin film is in-plane stress state along the film surface. In Eq. (10), E is the elastic modulus, σ is the in-plane stress, ν is Poisson's ratio, and ε_0 is the strain at $\psi = 0^o$
- From Eq. (10), ε_ψ exhibits a linear relationship with $\sin^2\psi$. The term $\frac{1+\nu}{E} \cdot \sigma$ corresponds to the slope of the linear function, while ε_0 corresponds to the intercept. Therefore, by measuring XRD patterns at different ψ angles (as in Fig. 2), calculating d_ψ from Bragg's law (Eqs. (1) and (2)), determining ε_ψ using Eq. (3), and plotting ε_ψ as a function of $\sin^2\psi$ (Fig. 4(b)), the in-plane stress can be obtained from the slope of the fitted line.

$$\sigma = \frac{E}{1+\nu} \cdot \text{slop} \quad (11)$$

- A negative slope indicates that the specimen is under in-plane compressive stress, whereas a positive slope indicates in-plane tensile stress [29].

4.3 Requirements and Experimental Setup

- To apply the $\sin^2\psi$ method, the material should be crystalline; furthermore, if the material can be treated as isotropic, the strain–stress relationship can be simplified. In addition, the selected diffraction plane must provide sufficient diffraction intensity so that reliable measurements can be obtained over a range of ψ tilt angles.
- In terms of instrumentation, the XRD system should be capable of performing conventional θ-2θ diffraction measurements. The setup must also allow the specimen to be tilted to the desired ψ angles. If direct specimen tilting is not possible, the measurements can alternatively be performed by appropriately adjusting the X-ray source and detector geometry to achieve the equivalent ψ tilt condition.

5. EXAMPLE: RESIDUAL STRESS ANALYSIS OF THIN FILMS

5.1 Residual Stress Measurement of $Pb(Zr,Ti)O_3$ (PZT) Thin Films on a Flexible Metal-Foil Substrate

- In this section, we present an example of in-plane stress analysis for a polycrystalline PZT thin film deposited on a flexible metal-foil substrate by the sol–gel method.

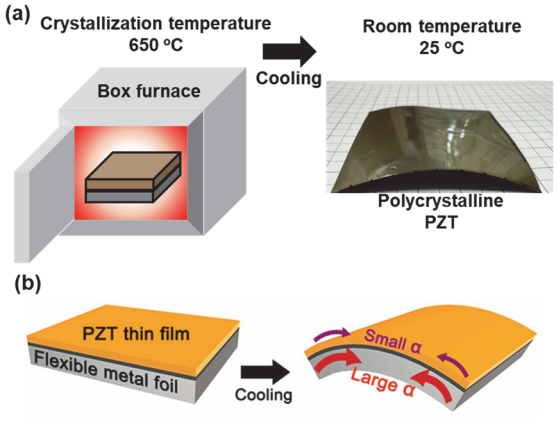

Fig. 5. (a) Schematic illustration of the crystallization process of a polycrystalline PZT thin film deposited on a flexible substrate and (b) schematic showing the mismatch in thermal expansion coefficients between the polycrystalline PZT thin film and the flexible substrate. Adapted with permission from [30]. Copyright 2019 Elsevier.

- As shown in Fig. 5(a), after crystallizing the sol–gel derived PZT thin film in a furnace at 650°C and subsequently cooling it to room temperature, in-plane stress is generated due to the mismatch in the thermal expansion coefficients between the flexible metal foil and the polycrystalline PZT film, as schematically illustrated in Fig. 5(b) [30].
- Accordingly, we demonstrate an analysis of the in-plane stress induced by the thermal expansion mismatch between the flexible substrate and the polycrystalline PZT thin film.
- Figure 6(a) shows a schematic of the θ-2θ scan geometry for out-of-plane XRD measurements of the polycrystalline PZT thin film. In this configuration, XRD analysis provides information on the lattice parameters and crystalline phases along the direction normal to the film surface.
- Figure 6(b) illustrates the θ-2θ scan geometry for measurements acquired with the specimen tilted by a ψ angle relative to the surface normal. In this case, XRD enables evaluation of ψ-dependent changes in d-spacing (i.e., strain), thereby capturing the effect of in-plane stress on the diffraction response.

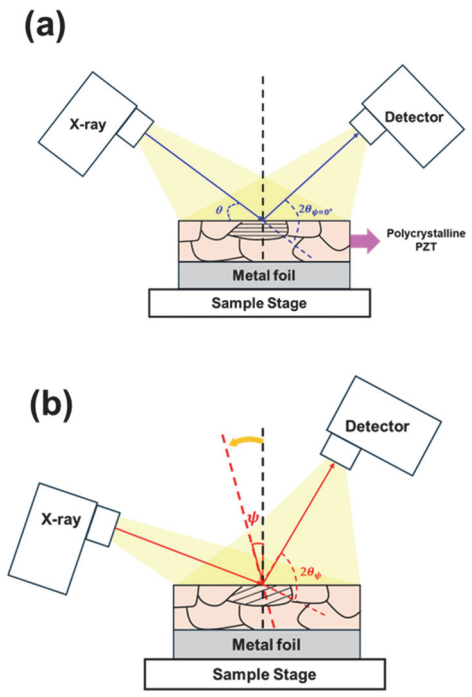

Fig. 6. (a) Schematic illustration of the θ-2θ scan geometry for a polycrystalline thin film and (b) schematic illustration of the scan geometry using the ψ tilt angle for a polycrystalline thin film.

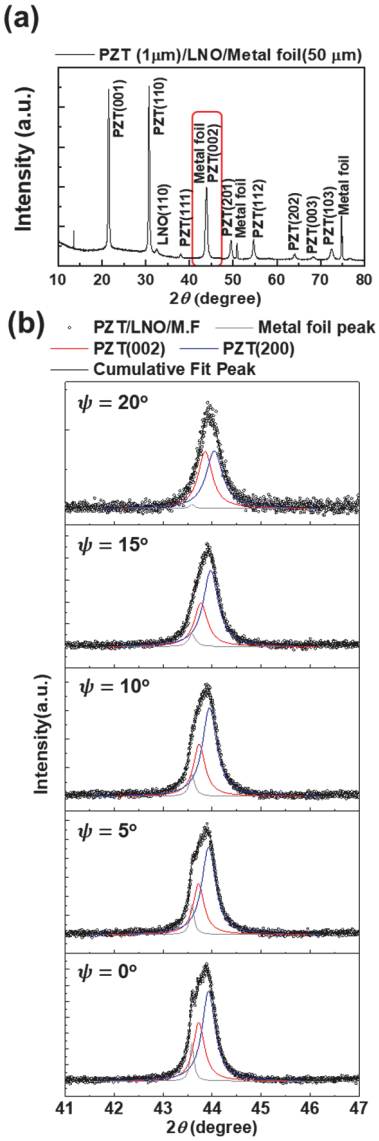

Fig. 7. (a) Out-of-plane θ-2θ XRD scan of a polycrystalline PZT thin film over the 2θ range of 10°–80°. (b) XRD scans in the 2θ range of 41°–47° acquired at ψ tilt angles of 0°, 5°, 10°, 15°, and 20°.

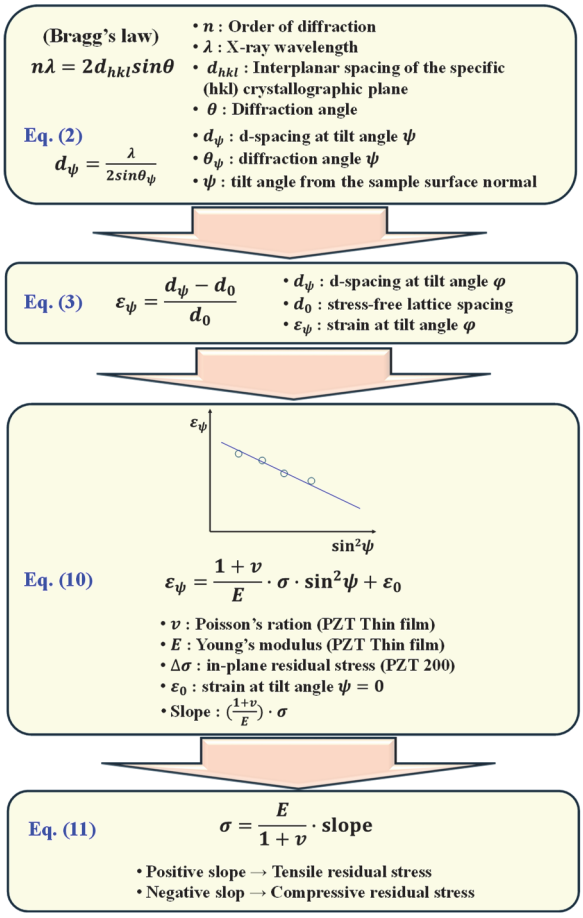

Fig. 8. Flowchart outlining the procedure for determining in-plane residual stress using the $\sin^2\psi$ method.

■ Figure 7(a) shows the θ-2θ XRD pattern obtained along the surface normal direction for the PZT thin film deposited on a flexible metal-foil substrate. From Fig. 7(a), the crystallinity of the polycrystalline PZT film and the lattice parameters along the out-of-plane direction can be confirmed.

■ Figure 7(b) presents XRD measurements of the polycrystalline PZT thin film on the flexible metal-foil substrate acquired at different ψ tilt angles (0°, 5°, 10°, 15°, and 20°) in the vicinity of the PZT⟨002⟩ reflection. Because the diffraction peaks from the metal-foil substrate overlap with the PZT(002) and PZT(200) peaks in this region, the peaks were separated through a multi-peak fitting procedure.

5.2 Calculation of In-Plane Stress Using the $\sin^2\psi$ Relationship

■ After completing the peak fitting as shown in Fig. 7(b), the quantities summarized in Table 3 can be obtained using Eqs. (2) and (3). The value of d_ψ is first calculated from Eq. (2). Using d_ψ together with d_0, the lattice strain ε_ψ is then determined from Eq. (3).

■ Figure 9 shows the linear ε_ψ–$\sin^2\psi$ plot constructed using the data in Table 3. Accordingly, the plot contains as many data points as the number of measured ψ angles. In general, a larger number of ψ angles improves the reliability of the linear regression.

Table 3. ε_{ψ} obtained from the change in PZT(200) peak according to the change in ψ angle using the $\sin^2\psi$ method.

ψ (degree)	$\sin^2\psi$	$2\theta_{\psi}$ PZT (200) (degree)	$2\sin\theta_{\psi}$	d_{ψ} (Å)	ε_{ψ}
0	0	43.9260 ± 0.0022	0.7480 ± 0.00004	2.0595 ± 0.0001	0.0202 ± 0.00004
5	0.00758	43.9273 ± 0.0023	0.7480 ± 0.00004	2.0596 ± 0.0001	0.0202 ± 0.00004
10	0.02985	43.9456 ± 0.0030	0.7483 ± 0.00005	2.0589 ± 0.0001	0.0198 ± 0.00004
15	0.06550	43.9693 ± 0.0045	0.7487 ± 0.00007	2.0578 ± 0.0002	0.0192 ± 0.00010
20	0.11249	44.0433 ± 0.0166	0.7499 ± 0.00027	2.0543 ± 0.0007	0.0176 ± 0.00034

Table 4. Slope of the linear function ε_{ψ}–$\sin^2\psi$ and in-plane residual stress obtained from the 2θ change of the PZT (200) peak according to the change in ψ angle.

Parameters	PZT (200)
Slope	−0.02252 ± 0.003
R^2	0.95
σ_{ψ} (GPa)	−1.21

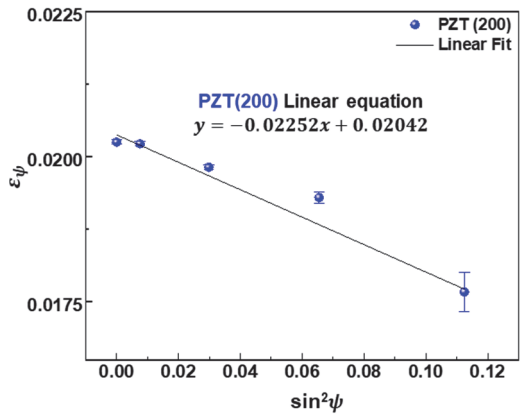

Fig. 9. Linear ε_{ψ}–$\sin^2\psi$ plot obtained from the ψ-dependent shift of the PZT(200) diffraction peak.

- As shown in Fig. 9, the data are fitted with a linear function. From the fitting results, a first-order relationship of $y = -0.02252x + 0.02042$ is obtained. The corresponding slope value and the goodness of fit, R^2, are summarized in Table 4.
- Using the slope of the ε_{ψ}–$\sin^2\psi$ plot together with the Young's modulus (E) and Poisson's ratio (ν) of the PZT thin film, the in-plane residual stress can be calculated from Eq. (11). In this analysis, E = 75 GPa and ν = 0.31 were used for the PZT film [31].

6. LIMITATIONS AND CONSIDERATIONS OF THE $\sin^2\psi$ METHOD

- If the specimen is not isotropic and exhibits a preferred crystallographic orientation (texture), the choice of diffraction planes available for different ψ angles can be restricted, which may introduce errors in strain measurements.
- In addition, because XRD has a shallow penetration depth (typically on the order of few micrometers), it primarily reflects stresses near the surface, and the through-thickness stress distribution cannot be resolved.
- Because the X-ray penetration depth is shallow, the measurement can be affected by near-surface conditions such as an oxide layer, surface contamination, or surface damage induced by mechanical processing.
- Due to limitations in the accessible ψ tilt range, it may be difficult to secure a sufficiently wide $\sin^2\psi$ span. Therefore, it is necessary to measure the d-spacing at a minimum of three ψ angles and to ensure a broad $\sin^2\psi$ range to improve the reliability of linearity assessment and slope determination [32].
- As ψ increases, diffraction peak intensity may decrease and peaks may broaden; thus, accurate peak fitting becomes increasingly important.
- Accurate alignment between the specimen surface and the XRD goniometer axis (half-cut alignment) is required [33]. If XRD measurements are performed without proper half-cut alignment, errors in the measured diffraction angle may occur, which can significantly affect the calculated residual stress.

7. CONCLUSIONS AND OUTLOOK

- This tutorial paper summarizes the XRD-based $\sin^2\psi$ method for quantitatively evaluating residual stress in functional polycrystalline thin films. We first outline the importance and origins of residual stress and compare nondestructive and destructive techniques, emphasizing the need for nondestructive analysis in thin-film systems. We then present a step-by-step $\sin^2\psi$ workflow based on ψ -tilt geometry and Bragg's law, linking d-spacing changes to lattice strain (ε_ψ) and linear ε_ψ–$\sin^2\psi$ regression, and summarize the procedure for determining in-plane stress from the slope using Young's modulus (E) and Poisson's ratio (ν).
- As a case study, a sol–gel derived polycrystalline PZT thin film deposited on a flexible metal-foil substrate was examined by tracking ψ -dependent peak shifts. After separating overlapping substrate and PZT(002)/(200) peaks via multi-peak fitting, $\sin^2\psi$ analysis revealed an in-plane compressive residual stress of approximately −1.21 GPa, primarily originating from thermal-expansion mismatch between the PZT film and the metal foil substrate. This result highlights the strong influence of thermal history and interfacial properties on residual stress in flexible substrate thin film devices.
- Finally, key limitations and practical considerations are discussed, including (i) restricted plane selection and potential errors in textured/anisotropic films, (ii) the shallow X-ray penetration depth that limits sensitivity to near-surface stress, (iii) reduced linearity and slope reliability due to a limited ψ range, and (iv) decreased peak intensity and peak broadening at higher ψ that demand robust peak fitting. Overall, the $\sin^2\psi$ method provides an effective nondestructive tool for diagnosing thin-film mechanical stability, and the workflow presented here offers practical guidance for stress management and reliability optimization in functional thin films, including flexible PZT devices.

ORCID

Chang Won Ahn https://orcid.org/0000-0003-0613-9823

ACKNOWLEDGEMENTS

This research was supported by Basic Science Research Program through NRF (RS-2023-00245221) and (RS-2023-00249613).

REFERENCES

[1] E. Fortunato, P. Barquinha, and R. Martins, *Adv. Mater.*, **24**, 2945 (2012). doi: https://doi.org/10.1002/adma.201103228

[2] K. J. Yu, Z. Yan, M. Han, and J. A. Rogers, *npj Flex. Electron.*, **1**, 4 (2017). doi: https://doi.org/10.1038/s41528-017-0003-z

[3] T. D. Lee and A. U. Ebong, *Renew. Sustain. Energy Rev.*, **70**, 1286 (2017). doi: https://doi.org/10.1016/j.rser.2016.12.028

[4] M. S. Kim, H. J. Lee, S. Behera, S. H. Cho, J. W. Jung, H. S. Kim, and I. D. Kim, *Adv. Mater.*, **38**, e15648 (2026). doi: https://doi.org/10.1002/adma.202515648

[5] M. Sheeraz, B. C. Park, and C. W. Ahn, *J. Korean Inst. Electr. Electron. Mater. Eng.*, **38**, 143 (2025). doi: https://doi.org/10.4313/jkem.2025.38.2.3

[6] S. J. Hyoung, E. S. Kang, Y. Kang, C. R. Kim, C. W. Ahn, B. W. Kim, J. S. Lee, and H. S. Han, *J. Korean Inst. Electr. Electron. Mater. Eng.*, **37**, 433 (2024). doi: https://doi.org/10.4313/jkem.2024.37.4.11

[7] G. Abadias, E. Chason, J. Keckes, M. Sebastiani, G. B. Thompson, E. Barthel, G. L. Doll, C. E. Murray, C. H. Stoessel, and L. Martinu, *J. Vac. Sci. Technol. A*, **36**, 020801 (2018). doi: https://doi.org/10.1116/1.5011790

[8] R. Koch, *J. Phys.: Condens. Matter*, **6**, 9519 (1994). doi: https://doi.org/10.1088/0953-8984/6/45/005

[9] L. B. Freund, *Int. J. Solids Struct.*, **37**, 185 (2000). doi: https://doi.org/10.1016/s0020-7683(99)00087-6

[10] A. G. Evans and J. W. Hutchinson, *Acta Metall. Mater.*, **43**, 2507 (1995). doi: https://doi.org/10.1016/0956-7151(94)00444-m

[11] W. D. Nix, *Metall. Trans. A*, **20**, 2217 (1989). doi: https://doi.org/10.1007/bf02666659

[12] U. Welzel, J. Ligot, P. Lamparter, A. C. Vermeulen, and E. J. Mittemeijer, *J. Appl. Crystallogr.*, **38**, 1 (2005). doi: https://doi.org/10.1107/s0021889804029516

[13] V. T. Srikar and S. D. Senturia, *J. Microelectromech. Syst.*, **11**, 206 (2002). doi: https://doi.org/10.1109/jmems.2002.1007399

[14] D. J. Miller, C. Proff, J. G. Wen, D. P. Abraham, and J. Bareño, *Adv. Energy Mater.*, **3**, 1098 (2013). doi: https://doi.org/10.1002/aenm.201300015

[15] P. J. Withers, Synchrotron X-ray Diffraction, in *Practical Residual Stress Measurement Methods* (John Wiley & Sons, Ltd, Hoboken, USA, 2013), p. 163.
doi: https://doi.org/10.1002/9781118402832.ch7

[16] M. Kim and O. Umezawa, *Metals*, **15**, 944 (2025).
doi: https://doi.org/10.3390/met15090944

[17] G. F. Harrington and J. Santiso, *J. Electroceram.*, **47**, 141 (2021).
doi: https://doi.org/10.1007/s10832-021-00263-6

[18] C. E. Murray and I. C. Noyan, Applied and Residual Stress Determination Using X-ray Diffraction, in *Practical Residual Stress Measurement Methods* (John Wiley & Sons, Ltd, Hoboken, USA, 2013), p. 139.
doi: https://doi.org/10.1002/9781118402832.ch6

[19] T. M. Holden, Neutron Diffraction, in *Practical Residual Stress Measurement Methods* (John Wiley & Sons, Ltd, Hoboken, USA, 2013), p. 195.
doi: https://doi.org/10.1002/9781118402832.ch8

[20] Y. Kang, Y. Qiu, Z. Lei, and M. Hu, *Opt. Laser Eng.*, **43**, 847 (2005).
doi: https://doi.org/10.1016/j.optlaseng.2004.09.005

[21] C. A. Taylor, M. F. Wayne, and W.K.S. Chiu, *Thin Solid Films*, **429**, 190 (2003).
doi: https://doi.org/10.1016/s0040-6090(03)00276-1

[22] C. Barile, C. Casavola, G. Pappalettera, and C. Pappalettere, *Sci. World J.*, **2014**, 487149 (2014).
doi: https://doi.org/10.1155/2014/487149

[23] G. S. Schajer, *J. Eng. Mater. Technol.*, **110**, 344 (1988).
doi: https://doi.org/10.1115/1.3226060

[24] G. S. Schajer and P. S. Whitehead, Hole Drilling and Ring Coring, in *Practical Residual Stress Measurement Methods* (John Wiley & Sons, Ltd, Hoboken, USA, 2013), p. 29.
doi: https://doi.org/10.1002/9781118402832.ch2

[25] X. Li, J. Liu, H. Wu, K. Miao, H. Wu, R. Li, C. Liu, W. Fang, and G. Fan, *Heliyon*, **10**, e28348 (2024).
doi: https://doi.org/10.1016/j.heliyon.2024.e28348

[26] M. R. Hill, The Slitting Method, in *Practical Residual Stress Measurement Methods* (John Wiley & Sons, Ltd, Hoboken, USA, 2013), p. 89.
doi: https://doi.org/10.1002/9781118402832.ch4

[27] J. Palma, R. Rivero, I. Lira, and M. François, *Meas. Sci. Technol.*, **20**, 115302 (2009).
doi: https://doi.org/10.1088/0957-0233/20/11/115302

[28] Bruker, *Residual Stress with XRD* (YouTube).
https://www.youtube.com/watch?v=eYDHb0gfDF8

[29] Q. Luo and A. H. Jones, *Surf. Coat. Technol.*, **205**, 1403 (2010).
doi: https://doi.org/10.1016/j.surfcoat.2010.07.108

[30] S. S. Won, H. Seo, M. Kawahara, S. Glinsek, J. Lee, Y. Kim, C. K. Jeong, A. I. Kingon, and S. H. Kim, *Nano Energy*, **55**, 182 (2019).
doi: https://doi.org/10.1016/j.nanoen.2018.10.068

[31] C. H. Hsueh, C. R. Luttrell, and T. Cui, *J. Micromech. Microeng.*, **16**, 2509 (2006).
doi: https://doi.org/10.1088/0960-1317/16/11/036

[32] A. Haase, M. Klatt, A. Schafmeister, R. Stabenow, and B. Ortner, *Powder Diffr.*, **29**, 133 (2014).
doi: https://doi.org/10.1017/s088571561400030x

[33] J. S. Choi, T. H. Kim, and C. W. Ahn, *J. Korean Inst. Electr. Electron. Mater. Eng.*, **35**, 431 (2022).
doi: https://doi.org/10.4313/jkem.2022.35.5.2